ARTICLE

Superior adhesion of graphene nanoscrolls

Hu Li [1], Raffaello Papadakis [2,3], S. Hassan. M. Jafri [1], Thomas Thersleff[1], Johann Michler[4], Henrik Ottosson[2,3] & Klaus Leifer[1]

An emerging material in the carbon family, a graphene nanoscroll (GNS) is composed of tubularly scrolled monolayer graphene and has shown superlubricity and large current sustainability, surpassing the properties of monolayer graphene itself. Here we report on the superior adhesion of GNS prepared with a high yield synthesis method that allows for mass production of high quality GNSs. Raman spectra indicate that the GNS still maintains the signature of monolayer graphene, implying the lacking of π-stacking between adjacent layers. Importantly, adhesion measurements using atomic force microscopy reveal these GNSs with height range of 120–130 nm show a 2.5-fold stronger adhesion force than pristine graphene. This result potentially indicates that the GNS has higher adhesion than monolayer graphene and even higher than the liquid–solid and hydrogen-bonding enhanced interfaces which are essential types of adhesions involved in the field of physical adhesions and thus, GNS could be a new candidate for super-strong and lightweight devices.

[1] Department of Engineering Sciences–Ångström Laboratory, Applied Materials Science, Uppsala University, Box 534, 751 21 Uppsala, Sweden. [2] Department of Chemistry–Ångström Laboratory, Uppsala University, Box 523, 751 20 Uppsala, Sweden. [3] Department of Chemistry–BMC, Uppsala University, Box 576, 751 23 Uppsala, Sweden. [4] Empa, Swiss Federal Laboratories for Materials Science and Technology, Laboratory for Mechanics of Materials and Nanostructures, CH-3602 Thun, Switzerland. Correspondence and requests for materials should be addressed to K.L. (email: Klaus.Leifer@angstrom.uu.se)

Adhesion plays an essential role in a large variety of processes in fields as different as biology, mechanical engineering, and thin film growth to name a few[1–6]. One of the most common adhesion mechanisms is physical adhesion which is also known as dispersive adhesion. It describes the tendency of disparate objects or surfaces to adhere to each other
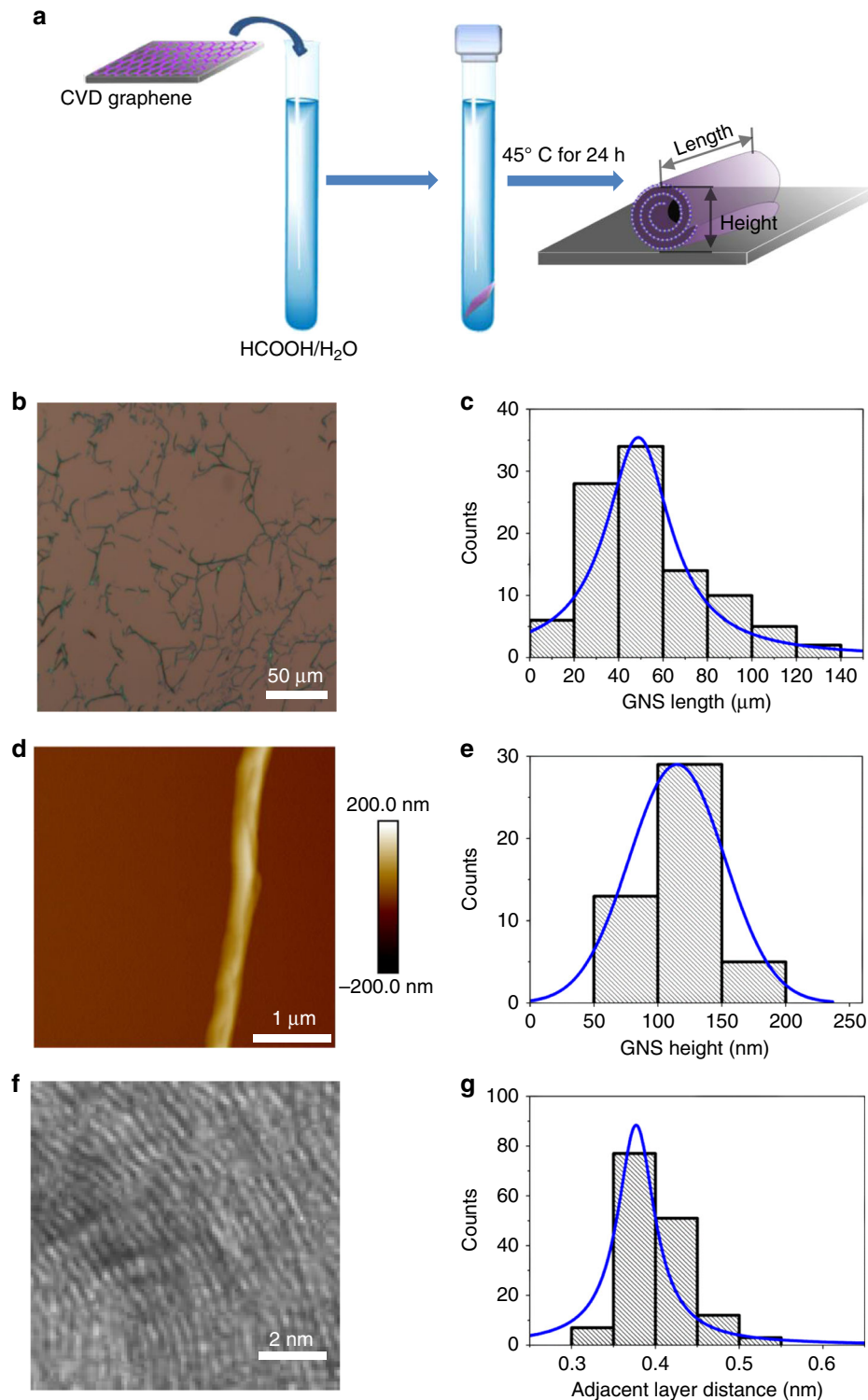

Fig. 1 Graphene nanoscroll (GNS) synthesis and characterizations. **a** A chemical vapor deposition grown graphene sample on SiO₂ (0.5 × 0.5 cm) was placed in a glass vial containing a freshly prepared 1/1 (v/v) HCOOH/H₂O mixture, in a way that the graphene sample was fully immersed in the aqueous HCOOH mixture. The vial was sealed with a rubber septum and degassed with Ar gas, then placed in an oil bath with a regulated temperature of 45 °C for 24 h. After this period, the graphene sample was repeatedly washed with water (to remove HCOOH) and then with acetone, and finally dried using a light stream of Ar gas. **b** Light optical image of the graphene nanoscroll (GNS) on SiO₂ substrate, where the lines are the GNS and the background is the SiO₂ substrate. **c** Length distribution diagram based on random 100 GNS. **d** AFM image of the GNS with a height of 125 nm. **e** Height distribution based on random 50 GNS. **f** A zoomed-in cross-section of a 125 nm high GNS, as well as (**g**) the statistic adjacent layer distance histogram (random 150 counts)
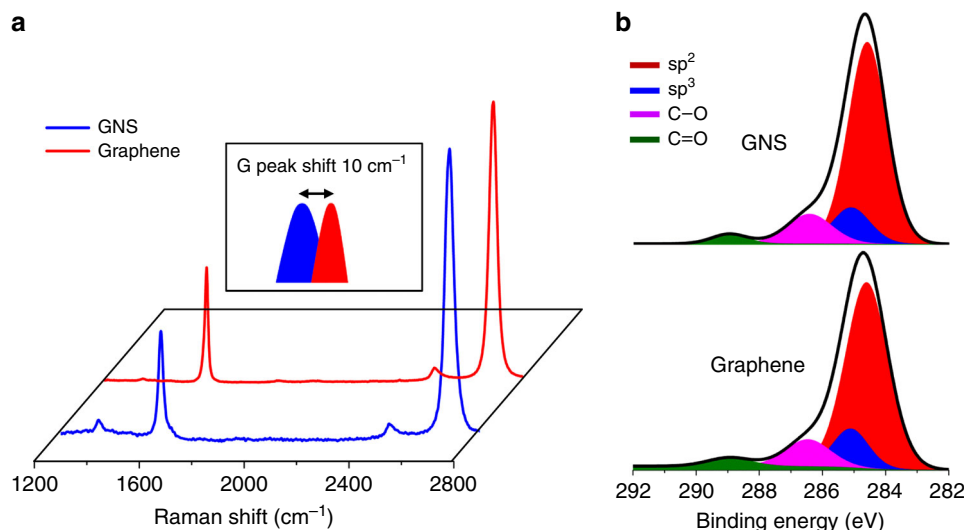
Fig. 2 Raman and X-ray photoelectron spectroscopy (XPS) characterization of the graphene nanoscroll (GNS). **a** Raman spectra comparison of pristine graphene and GNS. After spirally wrapped, the GNS shows the monolayer graphene featured spectra: sharp 2D band and $I_{2D}/I_G > 3$. (Inserted plot shows the left-shift of G band after scrolling up). **b** XPS of the C 1s peaks shows no chemical reaction observed during the fabrication, meaning that physical intercalation and rolling up should be the main synthesis mechanism

due to physical forces and is present in every type of adhesive. The strongest adhesions are normally observed at liquid–solid and hydrogen-bonding enhanced interfaces when only considering physisorption mechanisms[7,8]. Interestingly, comparably strong adhesion was observed on monolayer graphene due to its lattice strain[9–11], thereby generating considerable interest in the material for adhesion applications.

A graphene nanoscroll (GNS)[12–14], a relatively new member of the carbon family, consists of a continuous monolayer graphene[15,16] sheet with an open-ended and spirally rolled-up geometry, thereby exhibiting fundamentally different properties to other carbon materials. Theoretically, a GNS has a well-defined radius of curvature that would result in strain[17], which should lead to changes in the mechanical properties of the GNS compared to planar graphene. Even though carbon nanoscrolls have been first reported by Viculis et al.[12], and graphene-like nanoscrolls were discovered by Xie et al.[14], to date, there are only few publications that report on the experimental measurements of GNS properties. One of the main reasons is that the high yield and large quantity production of high quality GNS from monolayer graphene has not been reported. Here, we describe a synthetic process that can be used to produce high quantity and quality GNSs with the yield over 95%[12], which is calculated by counting the proportion of the scrolled area over the whole area through the optical microscopy image. This method thus has the potential to produce macroscopic quantities of the GNS with superior adhesion property, opening the way for novel material design such as molecularly intercalated carbon nanoscrolls.

Results

GNS synthesis and microscopic analysis. The synthesis of large quantities of GNS is achieved through a combination of chemical vapor deposition (CVD) graphene and appropriate mild synthesis conditions, namely aqueous formic acid at a temperature of 45 °C as shown in Fig. 1a. The rolling process of graphene results in more than 100 μm long GNS as it is observed in the light optical image (Fig. 1b) and the histogram gives an average length of 57 ± 12 μm (Fig. 1c). From the

evaluation of the light optical microscope image we measure that the surface coverage of the remaining graphene flakes on the surface is less than 5%, i.e., that the yield of the GNS synthesis method is over 95%. The AFM image in Fig. 1d demonstrates the formation of a long tubular structure. From the evaluation of AFM images of a large number of GNSs, we obtain an average height of 120 ± 35 nm shown in Fig. 1e. Combining the statistics of the heights and lengths, the GNS has an average aspect ratio of 500, placing it into the class of ultrahigh aspect ratio structures with a ratio of more than 300[18,19]. In order to investigate the inner structure of graphene nanoscrolls, transmission electron microscopy (TEM) cross-section is carried out and the corresponding high resolution TEM image is shown in Fig. 1f (also see Supplementary Note 1). Along with the GNS shell, the adjacent layer distances are measured and the average graphene layer spacing of 0.39 ± 0.03 nm is obtained (Fig. 1g), which is slightly larger than the graphite c-plane distance and matches well with reported values[12,14].

Raman scattering and X-ray photoelectron spectroscopy. The comparison of the Raman spectra of pristine graphene[20,21] and GNS (shown in Fig. 2a) demonstrates that the GNS has clearly maintained the graphene signature with the sharp 2D band (at ~2700 cm^{-1} with FWHM ~30 cm^{-1}) and the intensity ratio of more than three between the 2D band and G band (at ~1580 cm^{-1}). The sharp 2D band in GNS together with the absence of 2D band splitting reveals that the inner graphene layers lack π-stacking. The sharp 2D band signature is similar to that of monolayer graphene. Thus, the GNS in this work is significantly different from conventionally fabricated carbon nanoscrolls (CNS)[22,23]. The reason of the 2D band non-splitting phenomenon is mainly due to the deviation in the orientation from Bernal stacking[24], which has been observed during the deformation of multilayer graphene[25]. The increased c-plane spacing as compared to graphite could contribute to the observation of the graphene signature in the Raman spectra. The D band at 1350 cm^{-1}, normally indicating the presence of defects, is negligible in pristine graphene and has a slight increase in
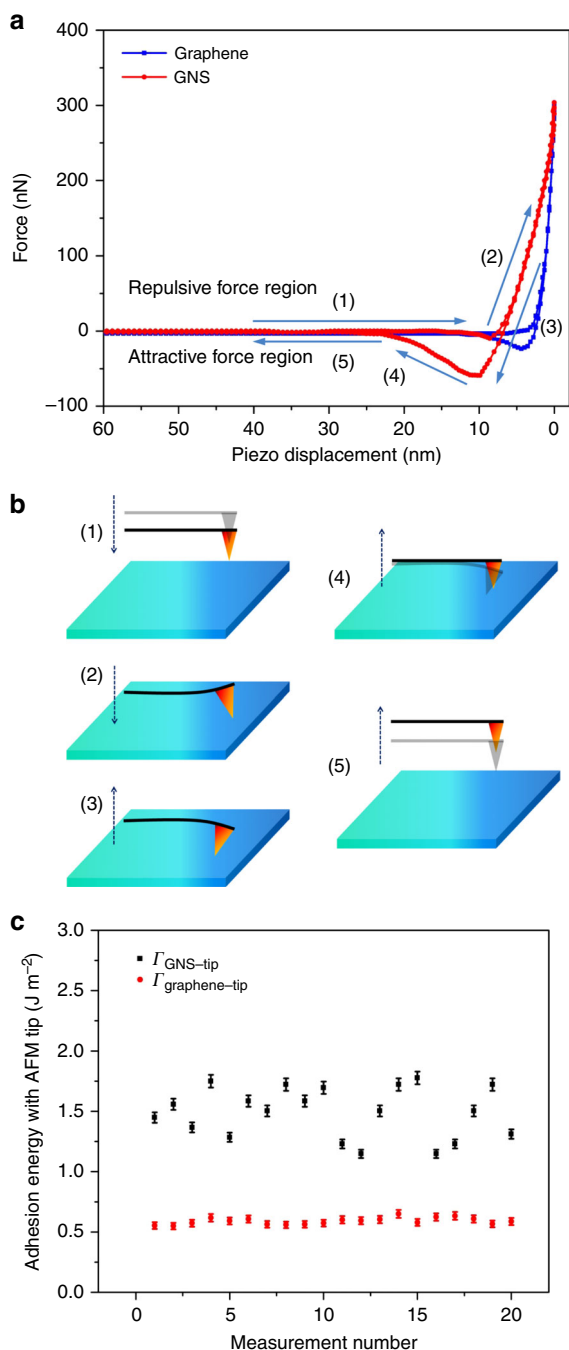
Fig. 3 Adhesion property measurement of the graphene nanoscroll (GNS) and monolayer graphene. **a** Typical force-displacement curve comparison of the GNS (red) and the monolayer graphene (blue). The displacement represents the movement of the piezo, where the displacement of zero is chosen at the highest load force. The indentation consists of five main phases shown in (**b**): (1) tip approaching towards the sample. (2) tip contacting and deforming the sample. In this phase, the force is repulsive. (3) tip retracting and the samples starts to recovery. At first, the force shows repulsive force and after the recovery of the sample, it turns to an attractive force. (4) tip jumping out of the sample. The jumping point refers to the maximum adhesion force between the sample and the tip. (5) tip retracting backwards the sample. **c** Adhesion energies between the AFM tip and the GNS and monolayer graphene with standard deviation as error bar. The measurements of the GNS are carried out on 20 different nanoscrolls with the height 120–130 nm

GNS. The G band, generated from the activation of the E_{2g} mode at the Γ points, shows a ~10 cm^{-1} low frequency shift in GNSs compared to pristine graphene (inserted graph in Fig. 2a), indicating a ~0.7%[26] in-plane strain in the GNS layers. X-ray photoelectron spectroscopy (XPS) was performed to investigate the chemical modification of the pristine graphene immersed in HCOOH/H$_2$O. The result as shown in Fig. 2b clearly shows that, before and after scrolling up, all peak areas, which correspond to different bonds, of pristine graphene and GNS remain nearly the same. This indicates that the synthesis mechanism is mainly a physical intercalation process and not a chemical reaction.

Adhesion measurements. Atomic force microscope based adhesion measurements are employed to investigate the adhesion properties of the GNS[27–32]. This method is based on the nanoindentation of a sharp AFM tip made of silicon into a surface, in which the force-displacement curves shown in Fig. 3a can be recorded and the graphic illustration of different phases is shown in Fig. 3b. In our experiments, the AFM based adhesion measurements are carried out on the GNSs with the height range of 120–130 nm. Comparing the force-displacement curves, GNS displays a 2.5-fold stronger adhesion force than pristine graphene for the same setpoint as used for the measurement on graphene, which is visible in phase iv of Fig. 3a. It is noted that the force curve has a slow recovery after the jump-off point, and it could be explained by the possible presence of capillary force[33] even if the experiments were carried out in a low humidity level of 20–27%. According to the work of Jiang et al.[34], the humidity level of less than 30% plays a limited role in the adhesion force measurements by using AFM technique, thus the obtained adhesion forces in our experiments should be reliable even if the low capillary force still exhibits an uncertainty. Another explanation of the slow recovery phenomenon is the possible delamination of the GNS layers, which needs to be further studied.

The Derjaguin-Muller–Toporov (DMT) model[35] is employed to determine the adhesion energy and can be expressed as (Supplementary Note 2):

$$F_{ad} = -2\pi R\Gamma \qquad (1)$$

where R is the AFM tip radius and Γ is the adhesion energy. The adhesion force F_{ad} is determined by the difference between the base force (zero force) and the minimum force and the extracted adhesion energies are shown in Fig. 3c. The measured adhesion energy between pristine graphene and AFM tip is $\Gamma_{graphene–tip}$=0.59 ± 0.03 J m^{-2}, while for GNS, we obtain a 2.5-fold increase of the adhesion energy to $\Gamma_{GNS–tip}$=1.49 ± 0.21 J m^{-2}. Using the derived adhesion energies above and the surface energy of SiO$_2$ (γ_{SiO2}=0.115 ± 0.2 J m^{-2}), the adhesion energy $\Gamma_{graphene–sio2}$ can be calculated to be 0.44 ± 0.02 J m^{-2}, indicating a good agreement between our measurement and references[9,34], while 1.12 ± 0.16 J m^{-2} is obtained for $\Gamma_{GNS–sio2}$ (Supplementary Fig. 1 and Supplementary Note 3). More control experiments (graphite, defected GNS and AFM tip with low spring constant) were performed and compared, which further confirm our measured adhesion results (Supplementary Figs. 2–4 and Supplementary Note 4 and Supplementary Figs. 4–6). This superior adhesion in GNS is potentially the highest reported value in the carbon family[9,36,37] (e.g., 0.45 J m^{-2}, 0.31 J m^{-2} and 0.33 J m^{-2} for graphene, graphite, and multiwall carbon nanotubes, respectively) and also implies that it is even higher than the liquid–solid and hydrogen-bonding enhanced interface adhesion energies in the field of physical adhesions[1,7,8]. This strong adhesion is also noticed when

we performed the sonication cleaning on both samples. After 5s sonication under the power of 75 W and frequency of 60 Hz, monolayer graphene on SiO$_2$ substrate is almost removed, while the GNS still remains in place.

Discussion

Based on the theoretical work of He et al.[10], the superior adhesion mechanism could be related to the strain in the graphene layer. They obtain a description of the adhesion of supported graphene calculating the total free energy of graphene using a continuum mechanics approach. Theoretically, the total free energy W_{total}[10,38] can be expressed as the sum of van der Waals potential energy W_{vdw}, intrinsic strain energy W_{in} (due to the lattice mismatch of graphene with substrate) and extra strain energy W_{strain} from the GNS synthesis process: $W_{total} = W_{vdw} + W_{in} + W_{strain}$. At the equilibrium state, the total free energy is negative, and the interface adhesion energy is described as: $\Gamma = -W_{total}$. Assuming the W_{vdw} and W_{in} are the same in GNS and pristine graphene, it can be deduced that the significant rise of adhesion energy in GNS is mainly attributed to W_{strain}. The lower adhesion of multilayer compared with single layer graphene was explained by the presence of strain in the single layer graphene[10]. Thus, since in the GNS case, we observe an increased strain as compared to the single layer, supported graphene, we can expect qualitatively that the adhesion energy of the GNS is higher. In fact, it could be shown theoretically that[17], in multilayer graphene, strain is built up by the curvature of the graphene layers. The curvature being the main difference between graphene and the GNS is most likely at the origin of the higher adhesion of the GNS. The geometry effect, especially the height of the GNS, may influence the adhesion energy of the GNS and, to further understand this, we have carried out adhesion measurements on thick (height 140–160 nm) and thin (height 40–60 nm) GNS, and the summarized result is shown in Table 1 (also see Supplementary Fig. 5 and Supplementary Note 7). Through the comparison, a higher adhesion of $1.72 \pm 0.12\, J\,m^{-2}$ was observed in the thicker GNS, while for smaller GNS, a comparable low adhesion of $0.62 \pm 0.02\, J\,m^{-2}$ was obtained. This result indicates that the adhesion energy of the GNS is height dependent, while even for the smaller GNS, it is still significantly higher than the adhesion energy of monolayer graphene. It is noted that other factors of extrinsic nature may also come into play and impact on the measured adhesion energy. However, the exact origin of the structural changes and how they specifically contribute to the adhesion in the system are still unknown to us and could be the topic for further studies.

In conclusion, we have reported a simple yet reproducible fabrication method to realize mass production of high quality GNS that preserves the Raman signature of monolayer graphene. By employing the AFM nanoindentation technique, a superior adhesion is observed in GNS, which is significantly larger than the adhesion of other carbon materials and even higher than adhesion at the liquid-solid and hydrogen-bonding enhanced interfaces. Adhesion is one of the key factors in determining the performance and reliability of the whole system[1], thus as a relatively new member in the carbon family, GNS with ultrahigh adhesion property has the potential to be used as an interfacial adhesion energy or to be directly incorporate in devices, also as a promising material for hydrogen storage[39]. The novel GNS synthesis method also provides an opportunity to synthesize new types of functionalized nanoscroll materials with molecular intercalation.

Methods

Materials. Monolayer Chemical Vapor Deposition (CVD) graphene on 1×1 cm silicon dioxide (285 nm)/silicon wafers was purchased from Graphene Super-market. The graphene was thermally grown on copper foils by standard CVD methods and then transferred to SiO$_2$/Si wafers under PMMA assistance[40,41]. The coverage of monolayer graphene was ~95% of the whole wafer and the samples were cut into 5×5 mm to fit the size requirement of the tube. Prior to experiments, the graphene samples were cleaned by immersing in chloroform for 24 h followed by a dry vacuum condition and the quality of the graphene film was checked through Raman spectroscopy, as well as X-ray photoelectron spectroscopy (XPS).

Table. 1 Measured adhesion energies of different carbon materials

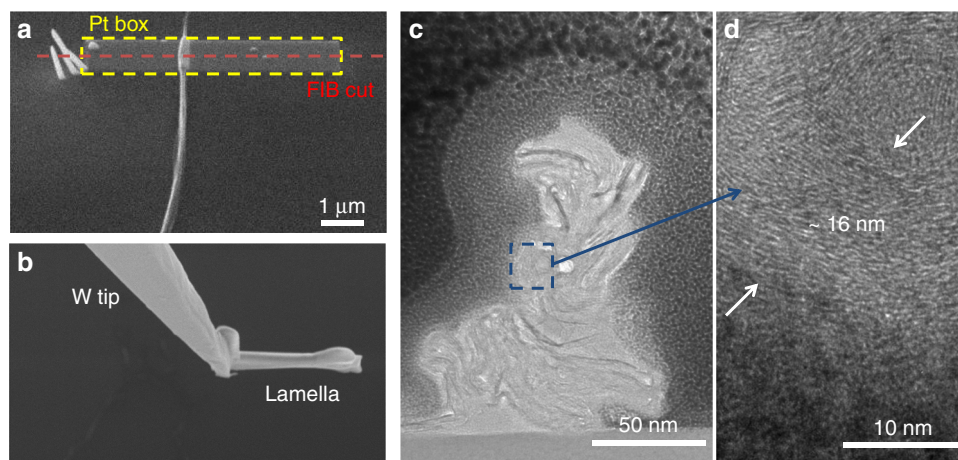| Sample	Adhesion energy ($J\,m^{-2}$)
Graphite	0.31
Graphene	0.44
Thick GNS (height 140–160 nm)	1.72
Major GNS (height 120–130 nm)	1.12
Thin GNS (height 40–60 nm)	0.62

Fig. 4 Transmission electron microscopy (TEM) cross-section preparation and observation. **a** Selected graphene nanoscroll (GNS) with 1 µm thick layer of Pt-C compound on top. **b** Scanning electron microscopy (SEM) image of the thin lamella attached to a tungsten nanomanipulator. **c** High resolution TEM image of the GNS cross-section. **d** zoomed-in TEM image of the GNS wall

Characterizations. Raman spectra of samples were recorded on Renishaw inVia confocal Raman microscope with the excitation wavelength of 532 nm. XPS was performed in Physical Electronics Quantum 2000 Scanning ESCA microprobe and the excitation source is a monochromatic Al K-Alpha X-ray (1486.7 eV). Optical images were recorded on an Olympus AX70 Research Microscope. AFM imaging and adhesion property measurement were carried out in a Bruker Multimode 8 AFM under PeakForce ScanAsyst (PF-ScanAsyst) mode and PeakForce Quantitative Nanomechanical Property Mapping (PF-QNM) mode, respectively.

Cross-section TEM imaging of the GNS. A 125 nm height GNS was chosen to prepare the cross-section of TEM imaging and a classic TEM lamella preparation was performed in FIB/SEM, FEI Strata DB235 as shown in Fig. 4. A 1 μm thick Pt-C layer was deposited on the GNS and then a thin lamella was obtained by focused ion beam milling and transferred to a copper grid. The lamella was finally polished and the cross-section observation was realized in a FEI Tecnai F30 TEM operated at 300 kV.

Adhesion measurements. The adhesion properties of pristine graphene and GNS were measured in an atomic force microscope Multimode 8 under Peak Force Quantative Nanomechanical Mapping (PF-QNM) mode. An antimony doped Silicon AFM tip with 8 nm radius (spring constant of 200 N m^{-1}) was utilized to acquire the force-displacement curves under the humidity of 20–27%. The tip radius is measured under the standard tip qualification process by using a rough titanium sample and the software NanoScope. A setpoint force of 300 nN was chosen for the adhesion measurements in order to avoid the possibility of plastic deformation on both of the AFM tip and SiO$_2$ substrate[42]. The measurements were carried under the piezo speed of 100 nm/s and the piezo noise of below 0.01 nm.

Data availability. The data that support the findings of this study are available from the corresponding author upon reasonable request.

References

1. DelRio, F. W. et al. The role of van der Waals forces in adhesion of micromachined surfaces. *Nat. Mater.* **4**, 629–634 (2005).
2. Hubbell, Ja, Thomas, S. N. & Swartz, Ma Materials engineering for immunomodulation. *Nature* **462**, 449–460 (2009).
3. Maboudian, R. & Carraro, C. Surface chemistry and tribology of mems. *Annu. Rev. Phys. Chem.* **55**, 35–54 (2004).
4. Dalva, M. B., McClelland, A. C. & Kayser, M. S. Cell adhesion molecules: signalling functions at the synapse. *Nat. Rev. Neurosci.* **8**, 206–220 (2007).
5. Yu, D. et al. Adhesion in flexible organic and hybrid organic/inorganic light emitting device and solar cells. *J. Appl. Phys.* **116**, 074506 (2014).
6. Li, H., Wani, I. H., Hayat, A., Jafri, S. H. M. & Leifer, K. Fabrication of reproducible sub-5 nm nanogaps by a focused ion beam and observation of Fowler-Nordheim tunneling. *Appl. Phys. Lett.* **107**, 103108 (2015).
7. Israelachvili, J. N. *Intermolecular and Surface Forces*. (Academic Press, Santa Barbara, 2011).
8. Maboudian, R. Critical review: adhesion in surface micromechanical structures. *J. Vac. Sci. Technol. B Microelectron. Nanom. Struct.* **15**, 1 (1997).
9. Koenig, S. P., Boddeti, N. G., Dunn, M. L. & Bunch, J. S. Ultrastrong adhesion of graphene membranes. *Nat. Nanotechnol.* **6**, 543–546 (2011).
10. He, Y., Chen, W. F., Yu, W. B., Ouyang, G. & Yang, G. W. Anomalous interface adhesion of graphene membranes. *Sci. Rep.* **3**, 2660 (2013).
11. Kim, S. & Ryu, S. Thickness-dependent native strain in graphene membranes visualized by Raman spectroscopy. *Carbon N. Y.* **100**, 283–290 (2016).
12. Viculis, L. M. A chemical route to carbon nanoscrolls. *Science* **299**, 1361–1361 (2003).
13. Berman, D., Deshmukh, Sa, Sankaranarayanan, S. K. R. S., Erdemir, A. & Sumant, A. V. Macroscale superlubricity enabled by graphene nanoscroll formation. *Science* **348**, 1118–1122 (2015).
14. Xie, X. et al. Controlled fabrication of high-quality carbon nanoscrolls from monolayer graphene. *Nano. Lett.* **9**, 2565–2570 (2009).
15. Geim, aK. & Novoselov, K. S. The rise of graphene. *Nat. Mater.* **6**, 183–191 (2007).
16. Papadakis, R. et al. Metal-free photochemical silylations and transfer hydrogenations of benzenoid hydrocarbons and graphene. *Nat. Commun.* **7**, 12962 (2016).
17. Zhang, D.-B., Akatyeva, E. & Dumitrică, T. Bending ultrathin graphene at the margins of continuum mechanics. *Phys. Rev. Lett.* **106**, 255503 (2011).
18. Yang, W. et al. Self-assembly of gold nanowires along carbon nanotubes for ultrahigh-aspect-ratio hybrids. *Chem. Mater.* **23**, 2760–2765 (2011).
19. Kharchenko, S. B., Douglas, J. F., Obrzut, J., Grulke, E. A. & Migler, K. B. Flow-induced properties of nanotube-filled polymer materials. *Nat. Mater.* **3**, 564–568 (2004).
20. Ferrari, A. C. & Basko, D. M. Raman spectroscopy as a versatile tool for studying the properties of graphene. *Nat. Nanotechnol.* **8**, 235–246 (2013).
21. Li, H. et al. Site-selective local fluorination of graphene induced by focused ion beam irradiation. *Sci. Rep.* **6**, 19719 (2016).
22. Sharifi, T. et al. Formation of nitrogen-doped graphene nanoscrolls by adsorption of magnetic γ-Fe2O3 nanoparticles. *Nat. Commun.* **4**, 2319 (2013).
23. Savoskin, M. V. et al. Carbon nanoscrolls produced from acceptor-type graphite intercalation compounds. *Carbon N. Y.* **45**, 2797–2800 (2007).
24. Slotman, G. J. et al. Effect of structural relaxation on the electronic structure of graphene on hexagonal boron nitride. *Phys. Rev. Lett.* **115**, 186801 (2015).
25. Gong, L. et al. Reversible loss of bernal stacking during the deformation of few-layer graphene in nanocomposites. *ACS Nano* **7**, 7287–7294 (2013).
26. Huang, M. et al. Phonon softening and crystallographic orientation of strained graphene studied by Raman spectroscopy. *Proc. Natl Acad. Sci. USA.* **106**, 7304–7308 (2009).
27. Lundstedt, A. et al. White-light photoassisted covalent functionalization of graphene using 2-propanol. *Small Methods* **1**, 1700214 (2017).
28. Dufrêne, Y. F., Martínez-Martín, D., Medalsy, I., Alsteens, D. & Müller, D. J. Multiparametric imaging of biological systems by force-distance curve-based AFM. *Nat. Methods* **10**, 847–854 (2013).
29. Bhushan, B. *Modern Tribology Handbook*. (CRC Press, 2001).
30. Cai, Y. et al. Biomineralization on single crystalline rutile: the modulated growth of hydroxyapatite by fibronectin in a simulated body fluid. *RSC Adv.* **6**, 35507–35516 (2016).
31. El-Sayed, R. et al. Single-walled carbon nanotubes inhibit the cytochrome P450 enzyme, CYP3A4. *Sci. Rep.* **6**, 21316 (2016).
32. Sun, F., Li, H., Lindberg, H., Leifer, K. & Gamstedt, E. K. Polymer fracture and deformation during nanosectioning in an ultramicrotome. *Eng. Fract. Mech.* **182**, 595–606 (2016).
33. Zitzler, L., Herminghaus, S. & Mugele, F. Capillary forces in tapping mode atomic force microscopy. *Phys. Rev. B* **66**, 1–8 (2002).
34. Jiang, T. & Zhu, Y. Measuring graphene adhesion using atomic force microscopy with a microsphere tip. *Nanoscale* **7**, 10760–10766 (2015).
35. Derjaguin, B. V., Muller, V. M. & Toporov, Y. U. P. Effect of contact deformation on the adhesion of particles. *J. Colloid Interface Sci.* **52**, 105–108 (1975).
36. Huang, R. Graphene: show of adhesive strength. *Nat. Nanotechnol.* **6**, 537–538 (2011).
37. Yu, M. F., Kowalewski, T. & Ruoff, R. S. Structural analysis of collapsed, and twisted and collapsed, multiwalled carbon nanotubes by atomic force microscopy. *Phys. Rev. Lett.* **86**, 87–90 (2001).
38. Fogler, M. M., Castro Neto, aH. & Guinea, F. Effect of external conditions on the structure of scrolled graphene edges. *Phys. Rev. B* **81**, 161408 (2010).
39. Mpourmpakis, G., Tylianakis, E. & Froudakis, G. E. Carbon nanoscrolls: a promising material for hydrogen storage. *Nano. Lett.* **7**, 1893–1897 (2007).
40. Li, X. et al. Large-area synthesis of high-quality and uniform graphene films on copper foils. *Science* **324**, 1312–1314 (2009).
41. Li, X. et al. Transfer of large-area graphene films for high-performance transparent conductive electrodes. *Nano. Lett.* **9**, 4359–4363 (2009).
42. Östlund, F. et al. Brittle-to-ductile transition in uniaxial compression of silicon pillars at room temperature. *Adv. Funct. Mater.* **19**, 2439–2444 (2009).

Author contributions

K.L. conceived the project. H.L., R.P., H.O., and K.L. designed the experiments. H.L. and R.P. synthesized the graphene nanoscrolls, as well as the control experiments. T.T. performed the cross-section of graphene nanoscrolls, as well as the following TEM imaging. H.L. and H.J. conducted the Raman, XPS, and adhesion property measurement

Additional information

Supplementary Information accompanies this paper at https://doi.org/10.1038/s42005-018-0043-2.

Competing interests: The authors declare no competing interests.

Reprints and permission information is available online at http://npg.nature.com/reprintsandpermissions/

Publisher's note: Springer Nature remains neutral with regard to jurisdictional claims in published maps and institutional affiliations.